High-Field Q Slope in Superconducting Cavities Due to Magnetic Field Enhancement at Grain Boundaries

J. Knobloch*, R. L. Geng, M. Liepe†, and H. Padamsee
Floyd R. Newman Laboratory of Nuclear Studies
Cornell University, Ithaca, NY 14853
†DESY, Notkestrasse 85, D-22603 Hamburg

Abstract

Quality (Q_0) degradation of superconducting, *field-emission-free* cavities at high accelerating gradient ($E_{\rm acc} >$ 20 MV/m) has been observed at a number of laboratories. This Q slope presents the main impediment to achieving gradients in excess of 25 MV/m needed for future superconducting high-energy accelerators. Presented here are Q_0 measurements and numerical simulations with SUPERLANS and ANSYS that provide insight into the mechanism responsible for the Q_0 degradation. A model, based on magnetic field enhancement at the grain boundaries, is developed and used to simulate the measured Q_0 results. It can explain differences in cavity behavior following 150 °C and 850 °C heat treatment. The model also explains a number of other observations, such as the improved cavity performance following electropolishing, and the predominance of cavity breakdown at the equator weld in chemically etched cavities.

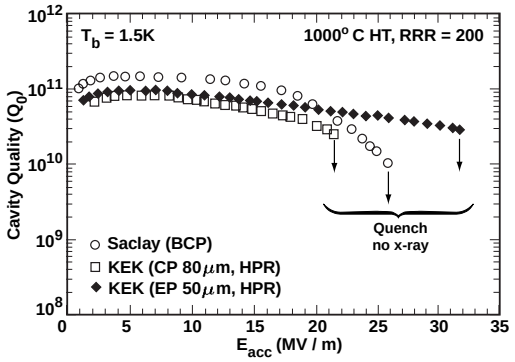

Figure 1: Quality of a single-cell TESLA cavity tested at Saclay (BCP treatment only) and subsequently electropolished and retested at KEK. The Q slope reduced and the breakdown field increased following electropolishing. *No x rays were detected*. From Reference [5].

1 INTRODUCTION

Until recently, thermal breakdown and field emission [1] proved to be the main limiting mechanisms in superconducting radiofrequency (rf) cavities. Both have now been eliminated—the former by postpurifying niobium, the latter by clean-room assembly and, in particular, high-pressure rinsing.

Interestingly, though, a steep decline of the cavity quality (Q_0) is still observed at high electric accelerating gradient ($E_{\rm acc}$), even in the absence of any field emission. The Q-drop in L-band cavities generally begins at about $E_{\rm acc} = 15$–20 MV/m with Q_0 a few 10^{10} and continues until the cavity breaks down at 25–35 MV/m with $Q_0 = 10^9$–10^{10}. Temperature mapping of such Q slope afflicted cavities revealed that the power dissipation occurs throughout most of the cavity [2]—in contrast to field emission which causes localized losses.

Thermometry also revealed that Q slope afflicted cavities etched with buffered chemical polish (BCP) frequently break down at the equator. [3, 4] Visual inspections of the breakdown region failed to locate any obvious weld defects. Repeated BCP treatment does shift the breakdown location *but only along the equator*. Yet, often no significant gain in breakdown field is achieved.

However, when electropolishing (EP) the cavity for about 50 μm or more the breakdown field increases, the Q slope decreases and the breakdown location shifts to a random location in the cavity. An example of this effect is shown in Figure 1. Repeated electropolishing may improve the cavity further. The maximum field achieved so far has been almost 40 MV/m with $Q_0 > 10^{10}$. [6] Subsequent BCP treatment in excess of a few tens of microns again reduces the gains achieved with EP.

A number of mechanisms have been proposed to explain the Q slope. They include the segregation of impurities and magnetic field enhancement at the grain boundaries.

In the former case it is stipulated that impurities segregate in the grain boundaries during BCP etching, which cause additional losses. In contrast to BCP, EP rounds and reduces surface features, possibly diminishing the extent of impurity segregation in the grain boundaries. Differences in acid composition between BCP (HF + H_3PO_4 + HNO_3) and EP (HF + H_2SO_4) may also lead to different impurity segregation.

The field-enhancement model assumes that the magnetic field locally exceeds the rf critical field $H_{\rm crit}$ due to field enhancement at microstructures on the rf surface. Primarily the boundaries between grains at different inclination are thought to be the source of the field enhancement. Again, BCP tends to accentuate these features. Although only a small region may quench, simply the sheer number of grain boundaries and the large normal-conducting surface resistance might explain the observed Q_0 reduction. Ultimately cavity breakdown is triggered by the most dissi-

* E-mail: jk30@cornell.edu

pative boundary. The reduced surface roughness of electropolished cavities in this case explains the diminished Q slope.

Preliminary studies of grain boundaries with a nuclear microprobe have failed to detect a consistently higher impurity concentration at boundaries than elsewhere. [7] We have therefore analyzed the Q slope based on the magnetic field enhancement at grain boundaries.

A scanning electron microscope (SEM) and a surface profiler were used to characterize the niobium surface following BCP and EP treatments. The magnetic field enhancement at such microstructures was then calculated with the electromagnetic code SUPERLANS. In conjunction, thermal simulations with ANSYS determined the temperature profile in the cavity wall in the presence of a normal conducting grain boundary. In particular the power dissipation and thermal stability of such a boundary was analyzed.

The results were combined to yield a numerical model which simulates the Q slope. This model was used successfully to reproduce the Q_0 versus $E_{\rm acc}$ curves of a cavity tested at Cornell following three different treatments which had had a marked effect on the Q slope.

2 CAVITY TEST RESULTS

Two high-RRR, 2-cell TESLA cavities were tested at Cornell with near identical Q_0 versus $E_{\rm acc}$ curves. One cavity was sent to KEK for electropolishing and further tests, the results being reported in [4]. The results of the other cavity are used here to illustrate the magnetic-field-enhancement model.

The cavity was produced from $1/16''$ Russian, RRR-500, niobium. The cells were deep drawn and electron-beam welded (full penetration from the outside) along the equator and irises. The following is the treatment and test history:

1. 150 μm removal with BCP 1:1:2 below 15 °C.
2. Cavity stored in clean air for one month.
3. High-pressure rinsed (HPR) twice at 1000 psi, one hour each time. Dried cavity in class 100 clean room for one day.
4. **Test A**.
5. Baked cavity on test stand (vacuum better than 10^{-6} torr) at 150 °C for ≈ 43 hours.
6. **Test B**.
7. High-pressure rinsed twice for a total of 110 min. Dried cavity in clean room for three days.
8. **Test C**.
9. High-pressure rinsed once for 50 min.
10. Heat treated in vacuum furnace for two hours at 880 °C.
11. High-pressure rinsed twice for a total of two hours. Dried in clean room for one day.
12. **Test D**.

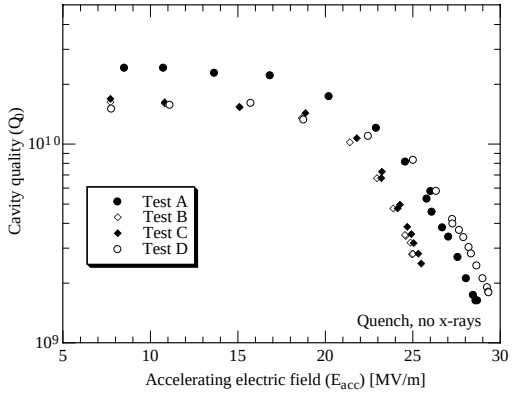

Figure 2: Q_0 measurements at Cornell with a chemically treated, RRR-500, two-cell TESLA cavity.

Table 1: Q_0 values measured at $\approx$ 1.7 K and 4.2 K at $E_{\rm acc} < 10$ MV/m. ℓ is the electron mean free path needed to achieve $Q_0(4.2\ {\rm K})$.

Test	$Q_0(\approx 1.7\ {\rm K})$	$Q_0(4.2\ {\rm K})$	ℓ
A	2.7×10^{10}	3.8×10^{8}	250 nm
B	1.7×10^{10}	6.5×10^{8}	16 nm*
C	1.7×10^{10}	6.5×10^{8}	16 nm*
D	$1.6 \times 10^{10\dagger}$	3.4×10^{8}	413 nm

* $R_{\rm BCS}$ using this value for ℓ only yields $Q_0(4.2\ {\rm K}) = 6.25 \times 10^8$.
† The bath temperature had not yet bottomed out when the measurement was taken. Higher Q_0 values may be possible.

High-peak-power processing was applied successfully in the tests, except for Test B, to eliminate *all* field emission. Figure 2 summarizes the results. Since some field emission remained in Test B, yet the results were identical to those from Test C, we know that the field emission in the former case was not the source of the Q slope.

Note the similar Q slopes in all tests. The most striking difference is the early onset of the Q slope and lower quench field following the 150 °C heat treatment between Tests A and B. The original Q slope is subsequently recovered after the 880 °C heat treatment.

The tests were all performed below 2.2 K. Precise measurements of the bath temperature ($T_{\rm b}$) were not carried out. However, we estimate $T_{\rm b} \approx 1.7$ K. Table 2 summarizes the 4.2-K and 1.7-K low-field Q_0 values. Of particular importance, as we will show later, is the the decreased 4.2-K BCS surface resistance following the 150 °C bake-out. We believe this can explain the early onset of the Q slope in Tests B and C.

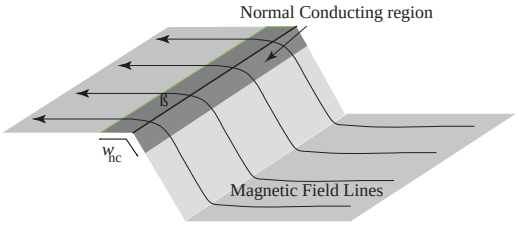

Figure 3: Schematic of a grain boundary that has quenched due to magnetic field enhancement at the grain boundary.

3 OUTLINE OF THE Q SLOPE MODEL

The remainder of the paper develops the field-enhancement model to explain the Q slope in general and in particular to simulate the results in Figure 2. We have chosen to concentrate on these results because the treatment history is well documented, and the *same* cavity was tested following various treatments that had a marked effect on the cavity behavior.

As mentioned in the introduction, a possible explanation of the Q slope is the quenching of grain boundaries due to the enhancement of the magnetic field above the critical rf field ($H_{\rm crit}$). It is well documented that the surface roughness of niobium treated with BCP can exceed 5–10 μm [8, 9], with abrupt changes in the slope between grains. The magnetic-field-enhancement factor $\beta_{\rm m}$ of a step will depend on geometry (angle, aspect ratio, radius of curvature at the corner ...) so that a distribution function $n_{\rm gb}(\beta_{\rm m})d\beta_{\rm m}$ is needed to describe the field-enhancement factors of all grain boundaries.

A grain boundary becomes normal conducting when $\beta_{\rm m}H = H_{\rm crit}$, where H is the surface-magnetic field in the absence of any surface roughness. A zeroth order estimate of the power dissipated per length ($\dot{Q}'_{\rm diss}$) by this normal conducting grain boundary is

$$\dot{Q}'_{\rm diss} \approx \frac{1}{2} R_{\rm nc} w_{\rm nc} (\beta_{\rm m} H)^2 \quad \text{if } \beta_{\rm m} H \geq H_{\rm crit} \tag{1}$$

which increases quadratically with H once the boundary quenches. Here $R_{\rm nc}$ is the surface resistance of normal conducting niobium and $w_{\rm nc}$ is the width of the region of the grain boundary that is in the normal state. Figure 3 illustrates the geometry of the grain boundary. Hence, as $E_{\rm acc}$ is raised, not only do more and more grain boundaries quench, but also the power dissipation in those that are already normal conducting increases. Eventually the most dissipative grain boundary causes cavity breakdown.

To estimate the total length $L_{\rm nc}$ of normal conducting grain boundaries needed to explain a Q_0 reduction from 2×10^{10} to 5×10^9 at $E_{\rm acc} = 30$ MV/m, we stipulate that $w_{\rm nc} \approx 1$ μm (a justification is given later). Since $R_{\rm nc}$ is much larger than the superconducting surface resistance $R_{\rm s}$, the area $w_{\rm nc} L_{\rm nc}$ is much less than the cavity surface area $A_{\rm cav}$ so that[1]

$$\frac{L_{\rm nc} w_{\rm nc} R_{\rm nc} H^2_{\rm crit}}{A_{\rm cav} R_{\rm s} H^2} = \frac{2 \times 10^{10}}{5 \times 10^9} = 4 \tag{2}$$

or

$$L_{\rm nc} = 4 \frac{A_{\rm cav} R_{\rm s}}{w_{\rm nc} R_{\rm nc}} \left(\frac{H}{H_{\rm crit}} \right)^2 . \tag{3}$$

For a 2-cell TESLA cavity $A_{\rm cav} = 0.156\,{\rm m}^2$, $R_{\rm s} = 13.8\,{\rm n}\Omega$ at $Q_0 = 2 \times 10^{10}$, $R_{\rm nc} = 1.35\,{\rm m}\Omega$ at 1.3 GHz and $H/H_{\rm crit} \approx 0.6$ at $E_{\rm acc} = 30$ MV/m ($H_{\rm crit} \approx 2000$ Oe). Hence

$$L_{\rm nc} = 2.3\ {\rm m}. \tag{4}$$

Given that the average grain is about 50 μm ($= l_{\rm gb}$) wide, there are roughly $A_{\rm cav}/l^2_{\rm gb} \approx 6 \times 10^7$ grains with a total grain boundary length of ≈ 6200 m. Hence only a small fraction of all grains need be normal conducting to explain the Q slope.

At this point we can identify two conditions placed on the distribution function $n_{\rm gb}(\beta_{\rm m})$. First, some grain boundaries must have $\beta_{\rm m} \geq H_{\rm crit}/H_1$, H_1 being the field at which the Q slope begins. If this occurs at $E_{\rm acc} = 20$ MV/m then the maximum occurring $\beta_{\rm m}$ has to be about 2.5. Second, at 30 MV/m $\beta_{\rm m} \approx 1.6$ is required to quench a grain boundary. Yet only a small fraction of the grain boundaries should be normal conducting at this field, as illustrated by (4). That is, $n_{\rm gb}(\beta_{\rm m})$ must peak below 1.6 and drop rapidly as $\beta_{\rm m}$ increases. The studies described below demonstrate that both conditions are consistent with BCP treated niobium surfaces.

If the distribution function and power dissipation due to a grain boundary are combined and integrated one can calculate the cavity losses as a function of $E_{\rm acc}$. These simulation results can then be compared directly with the measured Q_0 data.

Several important aspects of the Q slope model were investigated in detail and they are discussed more extensively in later sections.

1. How big are the surface features on BCP-treated niobium? How sharp are the transitions? Microscopy and profilometry have shown that 12 μm steps with slope angles on the order of 20° are possible. Most steps are smaller—about 5 μm in height. The corners of the steps have radii of curvature less than a few microns.

2. Are field-enhancement factors of 2.5, consistent with the onset of the Q slope, possible? What $\beta_{\rm m}$ values do the majority of the grain boundaries have? Are these less than 1.6? To answer these questions, we calculated the field-enhancement factors of steps found in Item 1 with the program SUPERLANS. The results indeed show that for structures on a BCP treated surface we can expect a maximum enhancement factor of 2.5 and an average $\beta_{\rm m}$ less than 1.5.

[1] We used the "effective" area which assumes a constant magnetic field throughout the cavity.

3. Having established that grain boundaries can quench at $E_{\mathrm{acc}} = 30$ MV/m, several more questions arise: Is a normal conducting grain boundary thermally stable, or does it immediately cause cavity breakdown? If not, how much power does the grain boundary dissipate? Are most losses due to the normal conducting region or do BCS losses contribute significantly? At what field does a normal conducting grain boundary trigger cavity breakdown?

   We explored these issues by simulating the thermal behavior of a normal-conducting grain boundary in superconducting niobium with the program ANSYS. These calculations have shown that grain boundaries with β_{m} up to about 2.5 indeed will only cause cavity breakdown at 30 MV/m and above—in agreement with our measurement results. Below the breakdown field, almost all power dissipation (for our cavity parameters) occurs in the normal conducting boundary rather than in the surrounding superconductor.

4. Our results thus confirmed that during cw cavity operation quenched grain boundaries are likely above about 20 MV/m. To complete the discussion we combined the information from Items 1–3 to arrive at an expression for the cavity Q_0 as a function of E_{acc}. This function was integrated numerically and compared with the measured Q_0 data discussed in Section 2. A good fit can be achieved for all tests by varying only one parameter—the critical magnetic field or, alternatively, the normal conducting surface resistance. A number of reasons are given why either of these (or both) may have changed between cavity tests.

4 SURFACE ROUGHNESS MEASUREMENTS

To gauge the microstructure of the the rf surface of a typical cavity, a number of niobium samples were polished with BCP and/or electropolished. These samples were studied in an optical microscope, an SEM, and with a surface profiler (Alpha Step 500 by Tencor) capable of resolving submicron steps. A more detailed report of these studies is given in [9].

The profiler's stylus has a 5 μm radius of curvature and a 60° shank angle. Hence, an abrupt step will be measured as an incline of 60° with a radius of curvature of 5 μm (see Figure 4) so that the surface profiles only yield an upper limit on these quantities. However, height differences are reproduced accurately.

Figure 5(a) depicts an SEM micrograph of RRR-300 niobium from Teledyne Wah Chang (not heat treated), following a 120 μm etch with BCP 1:1:2. A profile taken from this sample is shown in Figures 5(b) and (c). The largest surface features are about 12 μm high, while most features are about 5–10 μm in height. A smaller substructure exists on the grains. The root-mean-square height for all steps is about 5 μm. [9] SEM measurements at a glancing viewing angle also confirm this estimate of the step height.

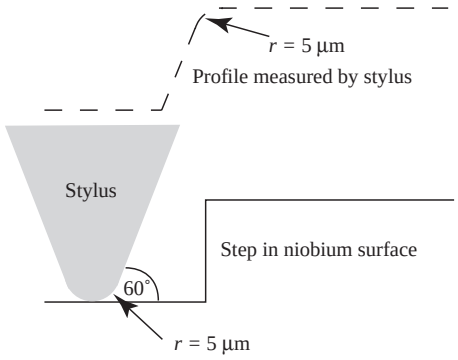

Figure 4: Schematic of a 90° step on a surface and the profile measured by the surface profiler.

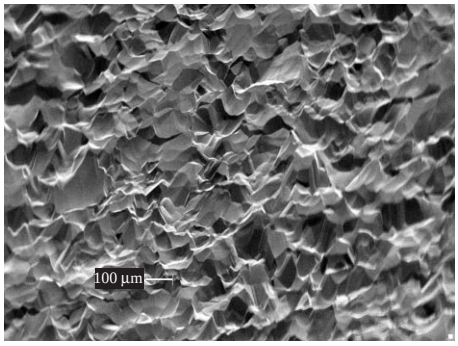

(a)

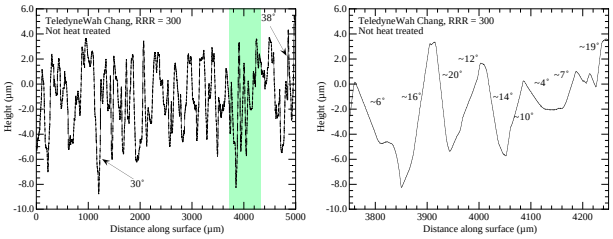

(b) (c)

Figure 5: Surface profiles of Teledyne Wah Chang, RRR-300 niobium (not heat treated), etched for 120 μm with BCP 1:1:2 below 15 °C. (a) SEM micrograph taken at a glancing angle (80°), but corrected for distortion. (b) 5000 μm profile scan, (c) 500 μm scan of the shaded region in (b). The angles indicate the slope angle at that point.

The graphs are deceptive regarding the aspect ratio of the surface features and the step angles due to the vastly different vertical and horizontal scales. In fact the measured slopes are usually very gentle, most of them being on the order of 5°–20°, with a maximum of slope of 40°. To *illustrate* this point, Figure 6 summarizes the slopes in scans from Figure 5(a). Only steps larger than a few microns were considered.

As mentioned above, these angles represent a lower limit on the slope angles. An additional complication in the eval-

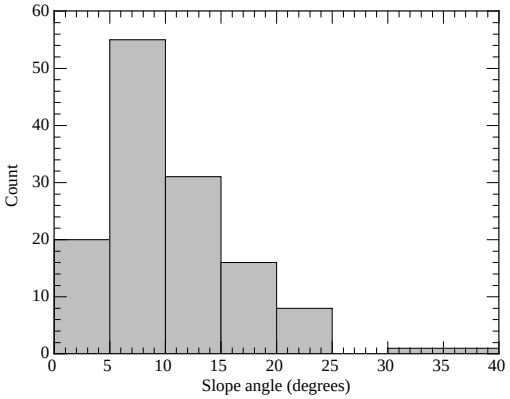

Figure 6: Histogram of the slope angles in Figure 5(b) and a similar scan. Only steps greater than a few microns were considered.

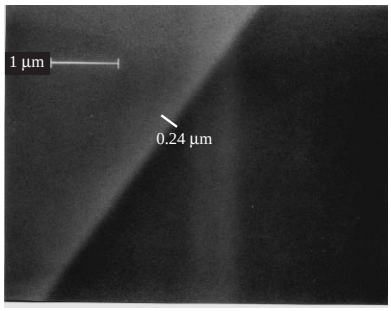

Figure 7: High-magnification secondary-electron micrograph of a grain boundary (viewed from straight above).

uation arises from the fact that the stylus' direction of travel need not always be perpendicular to the grain boundary. The measured angle θ_{meas} is related to the true angle (θ_{true}) by

$$\theta_{\text{true}} = \tan^{-1}\left(\frac{\tan\theta_{\text{meas}}}{\cos\alpha}\right) \tag{5}$$

where $90^\circ - \alpha$ is the angle the stylus motion makes with respect to the grain boundary. For example, if $\theta_{\text{meas}} = 20^\circ$ and $\alpha = 45^\circ$ then $\theta_{\text{true}} = 27^\circ$. Again this effect causes the slope angle to be underestimated.

To calculate β_{m}, some knowledge of the abruptness of the transition region between grains is also needed. As discussed above, the stylus' radius of curvature prevents a direct measurement with the profilometer. The only information gleaned from the results in Figure 5 is that generally the radius of curvature of the grain boundaries is less than 5 μm.

For a slightly better estimate one can use a high-magnification picture of a typical grain boundary, as in Figure 7. The contrast of secondary electron images is not only very sensitive to the surface composition but also the topography. Hence, surfaces sloping in different directions will appear with a different brightness. The transition between the two surfaces in Figure 7 is about 0.24 μm wide. If we make the assumption that one surface is a flat top and the other sloping at an angle θ, then for a normal viewing angle the apparent width of the transition region is $s = R\sin\theta$, R being the radius of curvature. If $s = 0.24$ μm as in Figure 7 and $\theta \approx 20^\circ$, $R = 0.7$ μm. If $\theta \approx 5^\circ$ then $R = 2.8$ μm. Hence radii of curvature of less than 3 μm are likely, especially if the transition region in Figure 7 is determined by the resolution of the SEM rather than its true width.

5 FIELD-ENHANCEMENT CALCULATIONS

Next we needed to estimate the field-enhancement factor of grain boundaries. To begin, we decided to concentrate on large steps (on the order of 10 μm) since our estimate in Section 3 suggests that only the biggest steps contribute to the Q slope.

5.1 SUPERLANS simulation geometry

We used an electromagnetic solver to calculate the fields inside a cavity in the presence of a small step on one of the walls. The ratio of the magnetic field in the presence of the step to that in the absence of the step then yields β_{m}.

The size (frequency) of the cavity has little impact on the calculated β_{m}, provided it is large enough so that the step does not affect the field distribution far from the step. Thus the cavity has to be much larger than the step.

Given that the step corner's radius of curvature is at most a few microns, a very high resolution mesh is needed near the step, and especially at the corner. The use of a fully 3-D code is very difficult due to the mesh requirement. Furthermore the shape of the corner has to be faithfully represented by the mesh. We therefore used the 2-D finite element code SUPERLANS (with cylindrical symmetry) whose mesh elements can follow the contours very well.

Which radius of curvature (R) does one end up using for the boundary? The considerations in Section 4 have demonstrated that $R < 3$ μm (more likely < 1 μm), but it could be considerably less than that. As R tends towards zero, β_{m} becomes infinite at the corner. How can we therefore trust the values for β_{m} that we calculate, since they depend on our choice of R? Fortunately, we can also place a reasonable lower limit on R to be used in the simulations. This value is based on the penetration depth of the rf field in the normal conducting niobium.

Once a grain boundary is fully normal conducting at the corner, the field penetrates the niobium a distance δ, known as the skin depth. Even if $R \ll \delta$, the rf field "sees" an effective radius of curvature (R_{eff}) at the corner on the order of δ. In the simplified view of an infinitely sharp corner depicted in Figure 8

$$R_{\text{eff}} = \frac{\delta}{\sqrt{2}-1} = 2.4\delta. \tag{6}$$

We used the normal-conducting penetration depth rather than the superconducting London penetration depth (λ_{L})

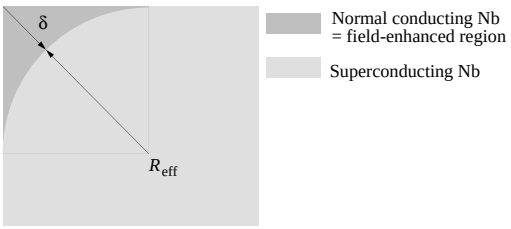

Figure 8: Geometry used to estimate the effective radius (R_{eff}) of curvature "seen" by the rf field at an infinitely sharp corner. δ is the skin depth of normal conducting niobium.

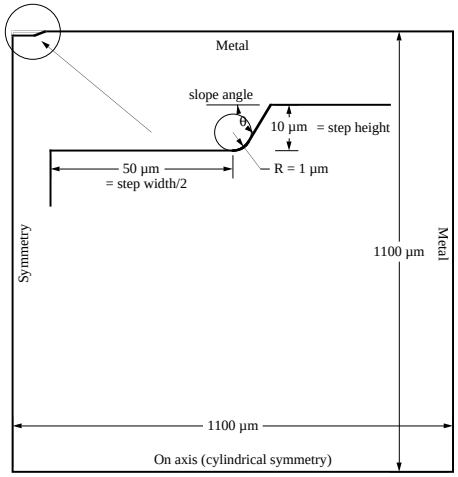

Figure 9: Pillbox cavity with a small step used for simulations in SUPERLANS. Calculations were done with the TE_{011} mode. Note the symmetry plane on the left boundary. The step is thus 100 μm wide.

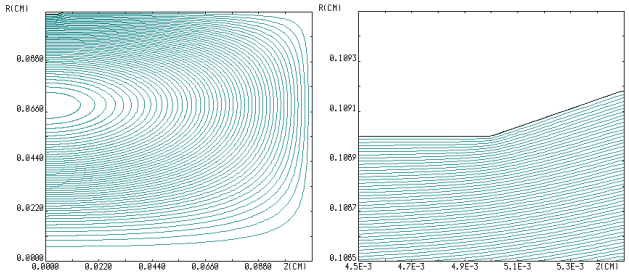

(a) (b)

Figure 10: Magnetic field lines of the TE_{011} mode in the cavity depicted in Figure 9. The step is 100 μm wide, 10 μm high, with a slope angle of 20°. (a) Complete cavity, (b) magnified view of the 10 μm × 10 μm region around the corner of the step.

for the following reason: λ_{L} is much smaller than δ (possibly even smaller than true radius of curvature R), and β_{m} is larger for $R_{\mathrm{eff}} \approx \lambda_{\mathrm{L}}$ than if $R_{\mathrm{eff}} \approx \delta$. When $\beta_{\mathrm{m}} H > H_{\mathrm{crit}}$ the grain boundary quenches, R_{eff} suddenly increases and β_{m} decreases. We suspect that the grain boundary thus enters a state similar to the intermediate state[2] (see, for example, [10]), where the grain boundary is partially superconducting and partially normal conducting. The superconducting portion decreases to zero until $\beta_{\mathrm{m}} H = H_{\mathrm{crit}}$, where here $\beta_{\mathrm{m}} \approx 2.4\delta$, i.e., the field enhancement is calculated for normal conducting niobium.

We therefore used R_{eff} based on δ in our simulations to determine when the grain boundary is completely normal conducting. However, future refinements of these simulations should probably include the finite conductivity of the niobium and the true radius of curvature.

At 1.3 GHz and 4.2 K, δ for niobium is about 0.3 μm. Equation 6 then yields $R_{\mathrm{eff}} \approx 0.7$ μm. In the calculations discussed below we chose $R_{\mathrm{eff}} = 1$ μm.

All calculations were done with a pillbox cavity and the TE_{011} mode, so the field in the absence of a step is known analytically. By placing the step at the center of the outer wall, as in Figure 9, we also ensured that (a) the magnetic field is perpendicular to the step and (b) the field is near uniform over the length of the step. The mesh at the corner was very dense (on the order of 0.1 μm or less, especially for shallow angles θ). Far away from the step, for example on axis, a mesh spacing as large as 70 μm was used.

5.2 *SUPERLANS results*

A simple test of SUPERLANS' ability to mesh and solve such small structures in a relatively large cavity, is to calculate the field enhancement of a perfectly conducting semicircle on the outside wall. The three dimensional analogy would be an infinitely long cylinder in a uniform magnetic field. This case is known analytically to have a field enhancement factor β_{m} = 2 at the top, independent of its size. [10] Using the geometry in Figure 9, we simulated a radius 1 μm rod (smaller than the steps used in the following simulations). SUPERLANS calculated β_{m} = 1.98—an agreement with the analytical result to within 1%.

Figure 10 depicts the magnetic field lines of the TE_{011} mode in the presence of a step. The field enhancement factor along the rf surface is given by the ratio of the calculated magnetic field to the field in the absence of the step. This ratio is depicted in Figure 11(a). The maximum field enhancement factor ($\beta_{\mathrm{m}}^{\mathrm{max}}$) for a number of different slope angles is depicted in Figure 11(b). Field enhancement values for the type of grain boundaries found on BCP treated surfaces can be as large as 2.5, the majority having β_{m} less than 1.5 ($\theta = 10°$).

One simulation was performed with a 100 μm × 10 μm step, slope angle 20° and a 5 μm radius of curvature. In that case $\beta_{\mathrm{m}} = 1.6$, which is not much less than the case with $R_{\mathrm{eff}} = 1$ μm (β_{m} = 1.8). The field enhancement model thus does not depend critically on our choice of R_{eff}.

Not only is the maximum β_{m} value of importance, but

[2] The *intermediate* state, which is due to geometry-dependent field enhancement, is not the same as the *mixed state* for type-II superconductors.

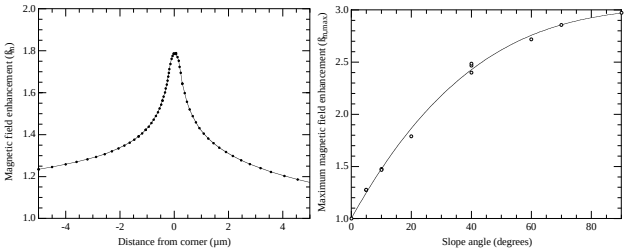

(a) (b)

Figure 11: Magnetic field enhancement due a $100\ \mu$m $\times$ $10\ \mu$m step. (a) Field enhancement along the rf surface near the corner (slope angle = 20°). (b) Maximum field enhancement versus slope angle.

also the width $w_{\rm nc}$ of the curve in Figure 11(a) needs to be determined. This information allows us to calculate the width of the quenched region about the grain boundary (recall, we used $w_{\rm nc} = 1\ \mu$m in Section 3). In our simple picture, only the very tip of the corner will quench when $\beta_{\rm m} H = H_{\rm crit}$. As H is increased further, the normal conducting region grows wider. We chose to "define" $w_{\rm nc}$ to be the width of the normal conducting region when $H = 110\%\, H_{\rm crit}/\beta_{\rm m}^{\rm max}$. For example, if a grain boundary quenches at $E_{\rm acc} = 20$ MV/m, the normal conducting width is equal to $w_{\rm nc}$ at 22 MV/m. In all cases shown in Figure 11(b), we found

$$0.5\ \mu{\rm m} < w_{\rm nc} < 0.75\ \mu{\rm m}. \qquad (7)$$

Since the width continues to increase with H we chose $w_{\rm nc} = 1\ \mu$m in the following simulations.

6 THERMAL SIMULATIONS

The discussions in the previous section establish that at least some grain boundaries on a BCP treated surface are likely to quench at field levels on the order of $E_{\rm acc} = 30$ MV/m (required $\beta_{\rm m} \approx 1.6$). The power dissipated by the grain boundary alone is then given by (1).

At this point it not clear, though, that the conduction of heat from such a line source by the surrounding niobium is sufficient to thermally stabilize the grain boundary. The situation is similar to that of a normal conducting particle that, if sufficiently large, can trigger thermal breakdown.

A simple criterion for thermal breakdown to occur is that the temperature at the particle (defect) radius must exceed the critical temperature of niobium ($T_{\rm c} = 9.2$ K). When this happens, the normal conducting region expands and a thermal runaway ensues. For RRR-300 material this situation occurs at 30 MV/m when the particle size is on the order of 15 μm.

For a spherical defect the temperature decrease rapidly as $1/r$, r being the distance from the defect.[3] In the case of an (infinitely long) line source of heat the decay of the temperature is much slower—it decays as $\ln(r)$ provided the thermal conductivity is temperature independent. Hence, even though $w_{\rm nc}$ is very small, it is not evident that a grain boundary which quenches will not immediately cause the cavity to break down.

[3]This model is very simplistic—it assumes that the thermal conductivity of the niobium is temperature independent.

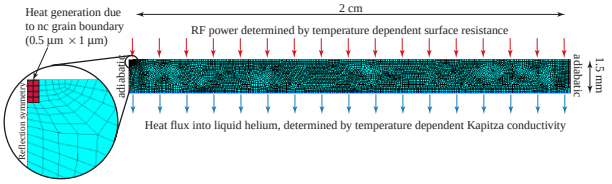

Figure 12: Geometry used in ANSYS simulations.

Another question is: Do the elevated temperatures near a grain boundary increase the BCS losses significantly so that the total losses attributable to a normal conducting boundary are augmented beyond $\dot{Q}'_{\rm diss}$ in (1)? In other words, do most of the losses occur in the grain boundary itself or are they due to the increased superconducting losses in the region near the boundary?

Both of these questions can be answered by numerically simulating the heat flow from a grain boundary in a slab of niobium. For this purpose we chose the finite element code ANSYS.

6.1 ANSYS simulation geometry

Although ANSYS is capable of 3-D simulations, so far we have performed all calculations with translational symmetry in the third dimension. Thus the normal conducting grain boundary is infinite in length. In future we hope to refine our calculations by using the full three dimensions.

Figure 12 depicts the simulation geometry and mesh. It consists of a 2 cm wide, 0.15 cm thick slab of niobium. The thickness was chosen to match that of the cavity used in our tests. Results from Reference [11] for RRR-500 niobium were used for the temperature-dependent thermal conductivity.

The line "defect" (cross section $1\ \mu{\rm m} \times 1\ \mu$m when symmetry is included) is situated in the high-density-mesh region at the top left hand corner. The power produced by this defect throughout its volume was determined with (1). The remainder of the top surface is a convective boundary, where the (temperature dependent) convection film coefficient is adjusted so that the power flux $\Phi_{\rm top}$ matches the superconducting rf losses:

$$\Phi_{\rm top} = \frac{1}{2} R_{\rm s}(T) H^2. \qquad (8)$$

Thus the model includes surface-resistance-dependent effects such as a global thermal instability.

The program SRIMP [12] was used to calculate the temperature dependent BCS surface resistance of niobium with a London penetration depth of 30 nm ($= \lambda_{\rm L}$) and a coherence length of 40 nm ($= \xi_{\rm c}$). [13] The mean free path

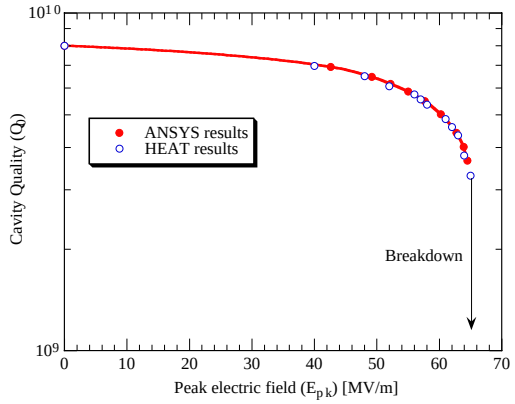

Figure 13: Comparison of global thermal breakdown simulations for a 3-GHz, RRR-400 cavity at 1.4 K.

ℓ was adjusted until $Q_0(4.2\text{ K}) = G/R_s(4.2\text{ K})$ equaled that in Table 2, G being the geometry factor (275 Ω for the TESLA shape). A residual resistance R_0 was also added at all temperatures so that $R_s(1.7\text{ K})$ yielded the low-temperature Q_0 values in Table 2.

Similarly, a convective boundary at the bottom permitted heat to flow into the helium bath. In this case the flux (Φ_{bottom}) is determined by the temperature dependent Kapitza conductivity $H_K\,(T_b, \Delta T)$:

$$\Phi_{\text{bottom}} = H_K(T_b, \Delta T)\Delta T, \tag{9}$$

where ΔT is the temperature difference between the niobium and the helium bath, and T_b is the bath temperature. We used the function

$$H_K\,(T_b, \Delta T) = 0.02\,T_b^{4.65} f(T_b, \Delta T) \tag{10}$$

$$f(T_b, \Delta T) = 1 + 1.5\tau + \tau^2 + 0.25\tau^3 \tag{11}$$

$$\tau = \frac{\Delta T}{T_b}, \quad \Delta T \le 1.4\text{ K}$$

quoted in Reference [14]. When ΔT is greater than 1.4 K, Φ_{bot} exceeds the critical heat flux for helium II ($\approx$ 1 W/cm^2) and the Kapitza conductivity is drastically reduced [15], in our case by a factor of 20.

The left and right boundaries are taken to be adiabatic (= reflection symmetry). The right boundary is sufficiently far from the defect to have little impact on the results.

To gain confidence in ANSYS we used the same geometry to calculate Q_0 versus E_{acc} for a RRR-400, 3-GHz, *defect-free* cavity up to the global thermal breakdown limit.[4] These calculations had previously been performed with the program HEAT [16]. The results, shown in Figure 13, demonstrate that the agreement is very good.

6.2 *ANSYS results*

Given a quench field of $H_{\text{crit}} = 2000$ Oe and $w_{\text{nc}} = 1$ μm, the power dissipated in the normal conducting region is

[4] I.e., no grain boundary heating was included.

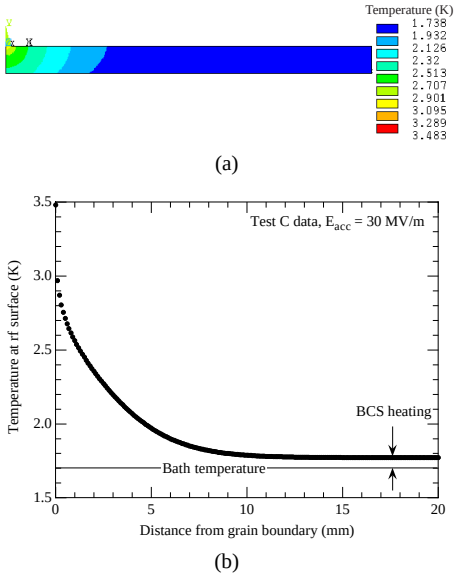

Figure 14: Temperature distribution within the niobium slab at $E_{\text{acc}} = 30$ MV/m with a grain boundary dissipating 17 W/m. (a) Complete slab, (b) temperature along the rf surface. All data calculated with surface resistance data for Test C.

$\approx 17 \times 10^{12}$ W/m^3 when $\beta_m H = H_{\text{crit}}$ (see (1)). Here we assumed that all the power is dissipated up to a depth of 1 μm (see Figure 12), so that the power dissipated per length of grain boundary is 17 W/m.

Figure 14 depicts the temperature profile in the slab at $E_{\text{acc}} = 30$ MV/m for a grain boundary with $\beta_m = E_{\text{crit}}/E_{\text{acc}} = 1.62$, $E_{\text{crit}} = 49$ MV/m being the accelerating gradient when $H = H_{\text{crit}}$. Similar simulations were performed up to $E_{\text{acc}} = 33$ MV/m, and in all cases, just as in Figure 14, we found that the grain boundary is thermally stable. Thus, a boundary that quenches at $E_{\text{acc}} \le 33$ MV/m and dissipates 17 W/m will *not* cause thermal breakdown in a cavity *at the quench field of the boundary*. Its only effect is to reduce the Q_0.

A striking feature of Figure 14 is the width of the temperature distribution despite the relatively low peak temperature ($< T_c$). This fact is a consequence of the infinitely long line defect used in the simulation and can lead to a thermal runaway due to the BCS surface resistance. In reality grain boundaries range from about 50 μm to 1 cm in length, depending on the annealing history of the niobium. Hence the temperature distribution shown here will only apply up distances on the order of the length of the grain boundary. We will return to this observation later in the discussion of breakdown in Q slope-afflicted cavities.

In the absence of any superconducting losses, a normal conducting grain boundary simply dissipates $\dot{Q}'_{\text{diss}} = 17$ W/m at the boundary's quench field $E_q = E_{\text{crit}}/\beta_m$, irrespective of what E_q is. However, the superconducting losses of the surrounding niobium are also increased due to the presence of the quenched boundary, and the total losses

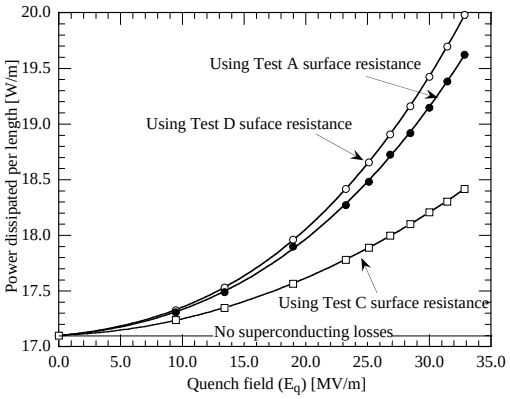

Figure 15: Total power dissipation due to a grain boundary quenching at field $E_{\rm q}$ ($\beta_{\rm m} = E_{\rm crit}/E_{\rm q}$). Superconducting losses increase the dissipation above 17 W/m. Subtracted out are the superconducting losses in the defect free case to yield the losses entirely attributable to the quenched boundary.

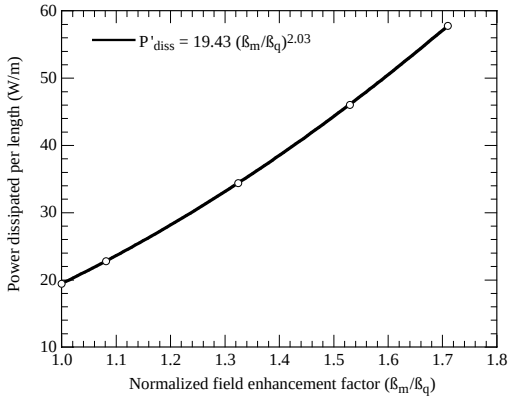

Figure 16: Power dissipated per length by a grain boundary as a function of $\beta_{\rm m}$ at $E_{\rm acc} = 30$ MV/m, relative to a grain boundary that quenches at $E_{\rm q} = 30$ MV/m with $\beta_{\rm q} = 1.63$. Superconducting losses in the defect free case have been subtracted out. The $R_{\rm s}$ data used here correspond to the Q_0 data from Test D.

attributable to the grain boundary ($P'_{\rm diss}$) exceed $\dot{Q}'_{\rm diss}$ by a field dependent amount.

Figure 15 depicts the total losses due to a normal boundary quenching at field $E_{\rm q}$.[5] The losses due to the superconducting surface resistance make up at most 15% of the total losses and are, not surprisingly, greatest for the case where the BCS resistance is largest at 4.2 K. Thus $P'_{\rm diss} \approx \dot{Q}'_{\rm diss}$.

Another question now arises: If a grain boundary quenches at $E_{\rm q}$, dissipating a power $P'_{\rm diss}$ given by Figure 15, how does that power increase as $E_{\rm acc}$ is raised above $E_{\rm q}$? And at what field does the cavity break down? Again, in the absence of BCS losses, the dependence is quadratic (see (1)).[6] Since superconducting losses matter fairly little in Figure 15, the deviation from (1) is expected to be small. Eventually, though, cavity breakdown will be triggered.

To make the Q slope calculation discussed later more convenient, we actually investigated how $P'_{\rm diss}$ changed with $\beta_{\rm m}$. I.e., if a boundary quenches with $\beta_{\rm m} = \beta_{\rm q}$ at $E_{\rm q}$, dissipating $P'_{\rm diss}$, how much more power does a grain boundary with $\beta_{\rm m} > \beta_{\rm q}$ dissipate at the same field?[7] Figure 16 demonstrates that indeed this power dissipation is (near) quadratic. The quadratic dependence continued up to a maximum $\beta_{\rm m} = 2.9$ at which point ANSYS no longer converged on a stable solution. We took this fact to indicate that thermal breakdown was occurring. At that point the temperature on the helium side, opposite the grain boundary, first exceeded 3.1 K and the heat flux was larger than the critical flux for helium II. Thus *breakdown was triggered by a lack of cooling at the helium interface, not a thermal runaway due to the BCS resistance.* This situation may, however, change for thicker niobium, different thermal-conductivity niobium, a higher bath temperature, or a different Kapitza conductance (which is difficult to measure accurately).

These results suggest that a grain boundary with $\beta_{\rm m}$ = 2.9 will cause cavity breakdown at 30 MV/m, dissipating $\dot{Q}'_{\rm diss} = 55$ W/m in the normal conducting region ($= 17\,{\rm W/m} \times (2.9/1.63)^2$). In fact, the width of the normal conducting region increases with field due to the distribution of $\beta_{\rm m}$ about the corner (see Figure 11(a)). A grain boundary at a field $E_{\rm acc} = 1.25 E_{\rm q}$ will typically have a width about twice that of $w_{\rm nc}$ which was determined at $1.1 E_{\rm q}$. Thus we really expect that a grain boundary with $2.9/\sqrt{2} = 2.1 < \beta_{\rm m} < 2.9$ will already quench the cavity at 30 MV/m. A 100 μm $\times$ 10 μm step with a 30°–40° slope thus is likely to be sufficient to explain the quench in the TESLA cavity tests at 30 MV/m. This grain boundary will have quenched at a field $E_{\rm q} \approx 1.63/2.5 \times 30$ MV/m $=$ 20 MV/m—close to the beginning of the Q slope in Figure 2.

7 SIMULATING MEASURED Q_0 DATA

At this point, the SUPERLANS and ANSYS simulation results can be combined to simulate the Q_0 versus $E_{\rm acc}$ results in Figure 2. Certain parameters in the model are not known precisely, such as the critical rf magnetic field ($H_{\rm crit}$) so we used reasonable estimates of these values. Hence, the following results should be considered more a feasibility study of the model rather than a rigorously quantitative result.

7.1 Total power dissipation in the cavity

To calculate the Q_0, the total power dissipation ($P_{\rm tot}$) in the cavity has to be determined. At low field, the superconduct-

[5] To arrive at these values, all simulations were repeated without the defect present. These determined the superconducting losses due to a defect free cavity (it turns out that the Q_0 is nearly field independent), which then were subtracted out from the losses calculated with the defect present.

[6] This statement must be modified if the increase of $w_{\rm nc}$ with H is taken into account.

[7] That grain boundary would have first quenched at $E_{\rm q}\beta_{\rm q}/\beta_{\rm m}$.

ing losses are the dominant source of power dissipation. At high field the grain boundaries dominate.

To determine the latter losses we need to know the number of grain boundaries at the rf surface. Given a cavity geometry factor $G = 275\ \Omega$ and the ratio of the peak surface magnetic field to the square root of the stored energy ($\kappa_H = 19506$ A/m$\sqrt{\text{J}}$), the effective area of the cavity is

$$A_{\text{cav}} = 2\frac{\omega}{G\kappa_H^2} = 0.156\ \text{m}^2 \tag{12}$$

provided we assume that the magnetic field is constant throughout the cavity.[8] Given (12),

$$Q_0 = \frac{2\omega U}{R_{\text{s}} A_{\text{cav}} H^2} = \frac{G}{R_{\text{s}}}. \tag{13}$$

in the absence of any defects.

The average length of a grain boundary in our cavity is about $l_{\text{gb}} = 50\ \mu$m so the total number of grain boundaries is

$$N_{\text{gb}} \approx 2\frac{A_{\text{cav}}}{l_{\text{gb}}^2} = 1.2 \times 10^8. \tag{14}$$

In fact, only half of these grains are outside step corners and lead to field enhancement. The other half are inside corners and reduce the magnetic field, thus playing no role in bringing about the Q slope. We will ignore the latter half in the following discussion by simply using

$$N_{\text{gb}} = 6 \times 10^7. \tag{15}$$

This value is needed to calculate the number of grain boundaries with magnetic field enhancement factor β_{m}, which in turn permits us to calculate the number of quenched grains at a given field.

The β_{m} distribution function $n(\beta_{\text{m}})d\beta_{\text{m}}$ presently is not known. However, the discussion in Section 3 has shown that the distribution function peaks below β_{m} = 1.6 and drops rapidly with increasing β_{m} to less than one part in 1000 at $\beta_{\text{m}} \approx 2.5$. Our surface profiles and SUPERLANS simulations are consistent with these constraints.

For our simulations we therefore chose

$$n(\beta_{\text{m}})d\beta_{\text{m}} = \frac{1}{\mathcal{N}} \exp\left(-\frac{|\beta_{\text{m}} - \beta_0|^{0.5}}{\sigma^{0.5}}\right), \tag{16}$$

where $\mathcal{N}$ normalizes the integral of $n(\beta_{\text{m}})$ to one. The "center" β_0 and "width" σ of the distribution are free parameters used to fit the model to the measured data. The main conditions placed on β_0 and σ are

$$\begin{aligned} \beta_0 &< 1.6 \\ \sigma &\ll 1. \end{aligned} \tag{17}$$

In addition, *once determined these values cannot change* unless the cavity undergoes some form of treatment (e.g., high-temperature heat treatment, electropolishing ...) that affects the structure of the rf surface. In the tests discussed in Section 2 this was not the case, so that the same β_0 and σ must be used to explain all Q_0 curves.

Given (16), the total number of grain boundaries with field enhancement factor β_{m} to $\beta_{\text{m}} + d\beta_{\text{m}}$ then is

$$N(\beta_{\text{m}})d\beta_{\text{m}} = N_{\text{gb}} n(\beta_{\text{m}})d\beta_{\text{m}}. \tag{18}$$

If all grain boundaries were perpendicular to the magnetic field then the total number of quenched boundaries at field E_{acc} would be

$$\begin{aligned} N_{\text{q}}(E_{\text{acc}}) &= N_{\text{gb}} \int_{\beta_1}^{\infty} n(\beta_{\text{m}})d\beta_{\text{m}} \\ \beta_1 &= \beta_{\text{min}} = \frac{E_{\text{crit}}}{E_{\text{acc}}}. \end{aligned} \tag{19}$$

For any other angle, only the perpendicular component of H is enhanced, so that the "effective" enhancement factor β_{eff} is given by

$$\beta_{\text{eff}} = \sqrt{\beta_{\text{m}}^2 \sin^2\gamma + \cos^2\gamma} \tag{20}$$

where γ is the angle between H and the grain boundary. The minimum angle (γ_{min}) at which a grain boundary with β_{m} will still quench at field E_{acc} thus is determined by

$$E_{\text{acc}}\beta_{\text{eff}}(\gamma_{\text{min}}) = E_{\text{crit}}. \tag{21}$$

For a random angular distribution of grain boundaries, the number of quenched grains then is

$$\begin{aligned} N_{\text{q}}(E_{\text{acc}}) &= \frac{2N_{\text{gb}}}{\pi} \int_{\beta_1}^{\infty}\int_{\gamma_1}^{\frac{\pi}{2}} n(\beta_{\text{m}})d\gamma\, d\beta_{\text{m}} \\ \gamma_1 &= \gamma_{\text{min}}. \end{aligned} \tag{22}$$

We require the power dissipated by all the normal conducting grain boundaries. A grain boundary that quenches at field level E_{q} dissipates a power $P'_{\text{diss}}(E_{\text{q}})$ per length, as given by Figure 15. Then, as the field is increased above E_{q}, the power dissipation of this grain boundary increases as $[\beta_{\text{eff}}E_{\text{acc}}/E_{\text{crit}}]^{2.03}$ (see Figure 16). Therefore the total power dissipated by all grain boundaries is

$$\begin{aligned} P_{\text{gb}} &= \frac{2P'_{\text{diss}}(E_{\text{acc}})l_{\text{gb}}N_{\text{gb}}}{\pi} \int_{\beta_1}^{\infty}\int_{\gamma_1}^{\frac{\pi}{2}} \left(\frac{\beta_{\text{eff}}(\gamma,\beta_{\text{m}})E_{\text{acc}}}{E_{\text{crit}}}\right)^{2.03} \\ &\times\ n(\beta_{\text{m}})d\gamma\, d\beta_{\text{m}}. \end{aligned} \tag{23}$$

Here we have assumed that the power dissipated *per length* by a grain boundary of length l_{gb} equals that of an infinitely long grain boundary. This approximation is not bad, since most of the power P'_{diss} is due to losses in the grain boundary rather than the surrounding superconducting niobium. However, this situation may change if the thermal conductivity, bath temperature, Kapitza conductivity, or wall thickness is changed. Full 3-D ANSYS simulations may then be required.

[8] This is not a bad approximation since the magnetic field is near uniform over most of the cell region.

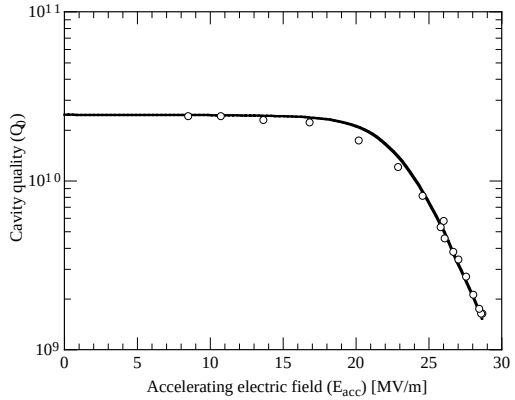

Figure 17: Comparison of the measured cavity quality (Test A) with that calculated by (25) using $H_{\rm crit} = 2000$ Oe.

The total power dissipation ($P_{\rm total}$) in the cavity is obtained by adding the superconducting losses in the absence of any grain boundaries ($P_{\rm sc}$).[9] Thus

$$P_{\rm total} = P_{\rm gb} + P_{\rm sc}, \tag{24}$$

and the cavity Q_0 as a function of field is

$$Q_0(E_{\rm acc}) = \frac{\omega U(E_{\rm acc})}{P_{\rm total}(E_{\rm acc})}. \tag{25}$$

7.2 Test A results

Equation 25 was integrated numerically using the program MATHCAD. The only free parameters in the model are β_0 and σ subject to the constraints in (17). In a sense, the critical magnetic field $H_{\rm crit}$ (or equivalently $E_{\rm crit}$) is also free since it is not known very well. We chose $H_{\rm crit} = 2000$ Oe ($E_{\rm crit} = 49$ MV/m) for Test A, which is in the range of accepted values for niobium.

A good fit, as shown in Figure 17, was achieved with $\beta_0 = 1.44$ and $\sigma = 0.0068$.[10] Note again that, to arrive at this fit, only β_0 and σ were varied. All other input data were obtained from the simulations discussed previously.

7.3 Effect of bakeout on rf properties

Mentioned earlier was the fact that non of the cavity treatments prior to Tests A–D should affect the distribution function $n(\beta_{\rm m})$. For our model to have any validity we must therefore be able to fit the other Q_0 curves using the same fit parameters. The only parameter that changes, it would appear, is the superconducting surface resistance (expressed via the Q_0 values at 1.7 K and 4.2 K). This results in minor differences in the values used for $P'_{\rm diss}$ (Figure 15) and in the losses calculated in the absence of any defects ($P_{\rm sc}$). The latter primarily changes the low field Q_0 values, but has negligible impact on the Q slope. Even the change of $P'_{\rm diss}$ cannot explain the relatively large differences in the Q slope between Test A and Tests B & C.

However, two aspects of the model have not yet been explored—namely the possibility that $H_{\rm crit}$ and $R_{\rm nc}$ need not be the same following the 150 °C bakeout.

The Q_0 results in Table 2 demonstrate that the bakeout increased the residual resistance, and more importantly reduced the BCS resistance by almost a factor of two. A similar effect following a 10-min, 300 °C bakeout was reported in Reference [17]. There it was found that the naturally occurring oxide layer on niobium (about 3 nm thick) begins to disintegrate above a bakeout temperature of ≈ 200–250 °C and diffuses into the bulk for several hundred nanometers with a temperature dependent diffusion constant

$$D_{\rm O} = 0.02 \exp\left(-\frac{13500\ {\rm K}}{T}\right)\ \frac{\rm cm^2}{\rm s}. \tag{26}$$

The effect of the oxygen rich layer was to *raise* the residual and normal conducting resistances, *lower* the BCS resistance, and *lower* the critical transition temperature ($T_{\rm c}$) by up to 6%. The observation that the BCS resistance reduces while $R_{\rm nc}$ increases is related to the fact that the BCS resistance scales inversely with the electron mean-free-path ℓ. [1] This fact was already noted in Table 2.

Similar results were obtained in Reference [18] with niobium wires. There it was found that $T_{\rm c}$ decreases by 0.93 K per atomic percent oxygen dissolved and the normal resistivity increases by 5.2 $\mu\Omega$ cm per atomic percent.

Since the thermodynamic critical field (and hence $H_{\rm crit}$) is proportional to $T_{\rm c}$ [1], we expect $H_{\rm crit}$ to reduce with increasing oxygen concentration.

A direct measurement of the impact of dissolved oxygen on $H_{\rm crit}$ and $R_{\rm nc}$ was made with a cavity that was first anodized and then heat treated to create an oxygen rich surface layer.[11] [20]

Similar to the Tests B & C, this cavity also had a high 4.2-K Q_0 (5.7×10^8) and its normal conducting Q_0 at 10 K was low—4×10^4 as opposed to 2×10^5 for BCP treated niobium. The breakdown field as a function of temperature is shown in Figure 18. The comparison with a cavity treated with BCP alone demonstrates that $H_{\rm crit}$ reduced significantly over the entire temperature range.

The bakeout prior to Test B was at a lower temperature, but lasted almost two days. An estimate of the diffusion length of the oxygen is given by

$$x(t,T) = \sqrt{2D_{\rm O}(T)t} \approx 0.1\ \mu{\rm m}, \tag{27}$$

which is greater than both the original oxide thickness and the London penetration depth of niobium ($\lambda_{\rm L} \approx 0.03\ \mu$m). Questions remain whether 150 degrees C heat treatment is sufficient to cause any of the oxide to disintegrate and further investigation is warranted.

However, another potential source of oxygen exists in this cavity: It has been shown that high-pressure rinsing at

[9] Recall that these losses were subtracted out when calculating $P'_{\rm diss}$, which includes only losses attributable to the presence of a normal conducting grain boundary.

[10] The fit was performed visually and may not be fully optimized.

[11] The technique used for this measurement is reported on in Reference [19].

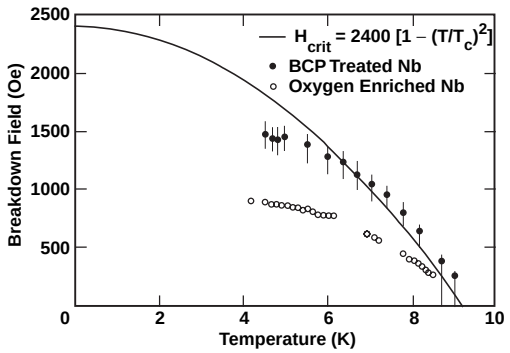

Figure 18: Measurement of the quench field in a cavity treated with BCP alone and one previously anodized and then heat treated to create an oxygen rich rf surface. [20]

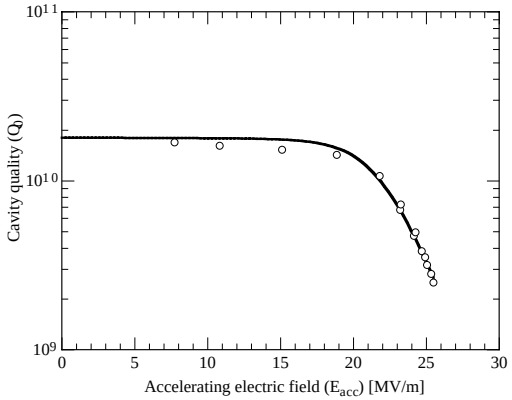

Figure 19: Comparison of the measured cavity quality (Test C) with that calculated by (25) using $H_{\rm crit} = 1875$ Oe.

1000 psi loads the niobium surface with oxygen [21] that may not be chemically bound and thus is free to diffuse at 150 °C. Since high-pressure rinsing is applied to all cavities that achieve high enough fields for the Q slope to manifest itself, the diffusion of oxygen during a low temperature bakeout may be unavoidable. Again further investigation is needed.

7.4 Test C results

Based on the discussion in the previous section, it seems reasonable that the critical magnetic field needs to be adjusted downward to fit the Test C results. The high $Q_0(4.2\ \mathrm{K})$ also suggests that the normal conducting surface resistance in (1) should be increased significantly, thereby raising $P'_{\rm diss}$. These effects combine to explain the worsening of the Q slope. Unfortunately, we did not measure the normal conducting Q_0 during these tests to substantiate the increased $R_{\rm nc}$. We thus ignored this aspect of the model and solely adjusted $H_{\rm crit}$.

$H_{\rm crit}$ now becomes the fit parameter, while β_0 and σ are the same as for Test A. Any change in $H_{\rm crit}$ here represents an *upper* limit, because $P'_{\rm diss}$ was kept constant.

Figure 19 demonstrates that a good fit can be achieved when $H_{\rm crit}$ is reduced from 2000 Oe to 1875 Oe, a 6% effect and consistent with the change in $T_{\rm c}$ reported in Reference [17] (and less than the change in Figure 18). On the other hand, if $H_{\rm crit}$ is fixed at 2000 Oe then $P'_{\rm diss}$ has to be increased by a factor of 2.7 for a reasonable fit of the Q_0 data. This increase is not unrealistic considering that the heat treatment of the anodized cavity caused the normal conducting Q_0 to decrease by a factor of five. In fact, the increase in $P'_{\rm diss}$, rather than the reduction of $H_{\rm crit}$, may be the dominant reason for the worsening of the Q slope following the bakeout.

The reduction of $H_{\rm crit}$ and any increase in $P'_{\rm diss}$ not only account for the change in the Q slope, but also explain why the cavity breakdown field reduced. If breakdown was caused by a particle we would not expect the field to reduce. In fact a slight increase is then likely because $Q_0(4.2\ \mathrm{K})$ improved. Furthermore, the rf surface was not exposed to particles during the heat treatment, so the lower breakdown field cannot be due a new particle on the surface. However, if $H_{\rm crit}$ reduces and $P'_{\rm diss}$ increases, the grain boundary with the largest $\beta_{\rm m}$ will quench at a lower field while also dissipating more power. Consequently it must precipitate cavity breakdown at a lower gradient, as observed.

7.5 Test D results

Following the 880 °C heat treatment, we expect the oxygen concentration at the rf surface to have reduced again as most of the oxygen diffused into the cavity bulk. The rf properties of the niobium in Test D should thus be similar to those during Test A. This is indeed borne out by the experiment. In fact, ℓ is larger ($Q_0(4.2\ \mathrm{K})$ slightly smaller) than for Test A, possibly because prior to Test A the cavity was exposed to clean air for close to a month. A thicker oxide may thus have been present on the rf surface, thereby reducing ℓ.

Based on this observation, we expect that if $H_{\rm crit}$ is at all different to that during Test A, it should be a little higher. In fact, $H_{\rm crit}$ had to be adjusted upward to 2070 Oe (3.5%) to be able to fit the data in Figure 20. Again, the change in $H_{\rm crit}$ represents an upper limit because we ignored any change in $R_{\rm nc}$.

Similar to the reduction of the cavity breakdown field in Tests B & C (with respect to Test A), an increased $H_{\rm crit}$ also explains the slightly higher breakdown field in Test D. Since the change in $H_{\rm crit}$ between Tests A and D is smaller than that between Tests A and C, one also expects the change in the breakdown field to be smaller. The experiments bear this fact out.

8 SUMMARY AND DISCUSSION

We have demonstrated that the magnetic field enhancement model to explain the Q slope is consistent with the observed properties of BCP treated niobium. A good fit

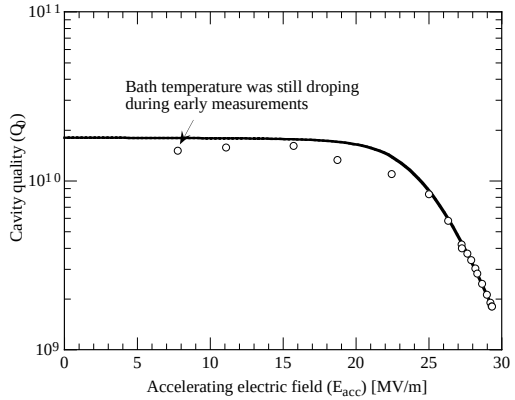

Figure 20: Comparison of the measured cavity quality (Test D) with that calculated by (25) using $H_{\rm crit} = 2070$ Oe.

of all the cavity test results discussed in Section 2 can be achieved with this model. In essence, $H_{\rm crit}$ is the only adjustable parameter, and it varies with the condition of the rf surface.

Other parameters, particularly the enhancement factor distribution function, are not known from experiment and thus have to be fit to the data using the Q_0 curves. However, once determined, *the same values were used to fit all three experimental curves*.

The SUPERLANS simulations demonstrated that the general features of the distribution function chosen for the fit (especially $\beta_0 \approx 1.4$) are consistent with the measured grain structure. Thermal stability of such a grain boundary when it quenches was shown with ANSYS to exist up to the field levels achieved in the cavity.

With increasing field, more and more grain boundaries quench, leading to the observed Q slope.

8.1 Uniform heating

The fraction of grain boundaries that are normal conducting at the maximum field achieved in each test is on the order of $5 \times 10^{-4} \ll 1$, in agreement with the estimate made in Section 3. Still, the total number of normal conducting grain boundaries is high, on the order 6×10^4 so that the average spacing between normal conducting grains is $\sqrt{A_{\rm cav}/(6 \times 10^4)} \approx 1.6$ mm. Each grain dissipates about $l_{\rm gb} \times 20$ W/m $= 1$ mW. The spacing between grains is too small and the individual power dissipation is too low for even the most sensitive thermometry systems to detect single normal conducting boundaries. [22] Rather, uniform heating throughout the high-magnetic-field region (most of the cavity) should be observed. Measurements at Saclay [2] have shown that this is indeed true. Future, high-sensitivity measurements should yield more information. When pushed to their limit, these may be able to detect the quenching of individual boundaries in cavities with large (millimeter-size) grains.

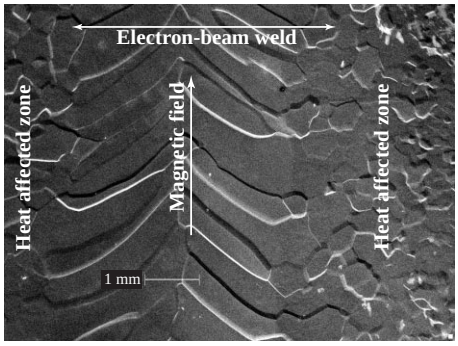

Figure 21: SEM micrograph of a full-penetration electron-beam weld as is used in superconducting cavities.

8.2 Breakdown field and location

The Q slope model can also explain the breakdown field and location in BCP treated cavities.

Cavity breakdown in the ANSYS simulations was triggered when a grain boundary no longer was thermally stable. In our case, this situation occurred when the flux at the helium interface exceeded the critical flux for helium II at about 30 MV/m. For thicker cavities, different thermal-conductivity niobium, or higher bath temperatures, breakdown may also be triggered by the temperature dependent BCS resistance. Further simulations are needed verify this statement.

Our ANSYS simulations were performed with infinitely long grain boundaries. For finite length grain boundaries we expect the calculated temperature profile to only hold within a distance less than the length of the boundary, i.e., about 50 μm. Beyond that distance, the line defect will begin to act more and more like a point defect, and the temperature drops rapidly.

The grains throughout most of the cavity are much smaller than the thickness of the cavity. It therefore is unlikely that they will trigger cavity breakdown due to the critical flux being exceeded at the helium interface.

However, the recrystallized grains along the equator electron-beam weld are more likely to cause breakdown for a number of reasons: First, they are several millimeters long [9]—greater than the cavity thickness—and hence act as near infinitely long line defects when viewed from the helium side. Second, the step height between grains tends to be large (perhaps 30 μm or more), greater than the steps in the remainder of the cavity. The $\beta_{\rm m}$ values in the equator region will therefore be relatively large. Finally, the grain boundaries in this region are *not* randomly orientated, but rather are near perpendicular to the magnetic field in the TM_{010} cavity mode generally used for acceleration. An example is shown in Figure 21. The power dissipation thereby maximized at these steps, and we expect the breakdown field predicted by ANSYS with infinite grain boundaries (≈ 30 MV/m) to apply to our rf cavity.

A cavity that has no significant particulate defects or inclusions will most likely break down at one of the large

equator-weld grain boundaries. Thermometry was not performed with the TESLA cavity discussed here. However, other measurement have shown that BCP treated cavities quench at the equator weld despite the absence of any obvious defect (e.g., a particle or an inclusion). Repeated BCP treatment shifts the breakdown location, but only along the equator. [3, 4] This observation supports the claim that breakdown is not triggered by a foreign defect but rather by a grain boundary. Repeated etching changes the individual grain boundaries so that a different one will dominate each time, yet still the most dissipative ones are always located along the equator.

Thermometry tests with seemless cavities could be used to verify this theory. In that case, the breakdown location should not be preferentially on the equator.

Note that the large equator grains primarily affect the breakdown field, but have little impact on the general Q slope, because only a very small percentage of the total grains are in the weld region. Seemless cavities are therefore not immune to the Q slope.

8.3 Electropolishing as a Q slope cure

Treatments that affect the surface morphology will alter the Q slope and the cavity breakdown field. In this case the change is due to a modification of the β_{m} distribution function rather than H_{crit} and R_{nc} as in our tests.

Electropolishing, which is known to produce very smooth, shiny surfaces, has been used successfully to reduce the Q slope and increase the breakdown field. [4, 5] In this manner, up to $E_{\mathrm{acc}} = 40$ MV/m has been achieved. [6]

Electropolishing a previously BCP treated cavity reduces the surface roughness gradually, with saturation in some cases only setting in after as much as 100–150 μm material removal. [8, 9] Substantial electropolishing is therefore needed before a significant improvement of Q slope is achieved.

The equator-weld grains will no longer have the dominant field enhancement factor and the cavity breakdown location may now be elsewhere. Experiments have shown this to be true. [23] It is quite possible that very small particles rather than a grain boundary are then the source of breakdown, indicating that still better cleaning techniques are needed to reach higher fields. At 40 MV/m 10 μm particles can cause breakdown. [24]

Not surprisingly, if an electropolished cavity is subsequently treated with BCP the surface roughness increases again and the Q slope worsens. The cavity breakdown field also is reduced. Saturation of the effect sets in after about 100 μm material removal. [5, 8] Once more this is in agreement with the observed saturation of the surface roughness after about 100–150 μm of BCP etching. [8]

8.4 Final remarks

One could conceive other models based on, for example, the segregation of impurities in grain boundaries during BCP treatment. Since electropolishing uses different acids, contamination may be avoided in that case. Intergranular losses or grain boundary quenches then bring about the Q slope, so that a similar approach as outlined in Section 7 might be used to calculate Q_0 data. However, why would one have to electropolish the rf surface for up to 100 μm before the Q slope disappears. Why does a light BCP etch ($< 10\,\mu$m) following electropolishing not cause the Q slope to reappear? With this model, the correlation between surface roughness and the Q slope would then just be coincidence.

The large variety of experimental observations that are consistent with the predictions of the field-enhancement model therefore strengthen it. These predictions form the basis for future experiments that we hope to perform in order to check the model's validity and to help us refine it.

A number of these experiments have already been discussed. For example, one should test the same cavity following a greater number treatments that alter the rf properties while maintaining the same distribution function for β_{m}. Even better would be a direct measurement of the distribution function (including the simulation of enhancement factors with finite conductivity niobium). Perhaps then a better fit of the Q_0 curves, especially at the beginning of the Q slope, can be made. A measurement of H_{crit} and R_{nc} following different cavity treatments would also be very useful. These parameters then are no longer free and the model is further constrained. Three dimensional simulations of quenched grain boundaries and field-enhancement factors would add another level of refinement.

Other questions include: How does the normal conducting width w_{nc} change with field? How does such a normal conducting–superconducting system behave at the boundary? How does the average grain size affect the Q slope? How does the cavity thickness, the RRR, and the bath temperature affect the Q slope and the breakdown field? Can the reduction of the Q slope following electropolishing be explained solely by the smoothing of the rf surface? ...

9 REFERENCES

[1] H. Padamsee, J. Knobloch, and T. Hays, *RF Superconductivity for Accelerators,* Wiley and Sons, New York, 1998.

[2] H. Safa, High gradients in scrf cavities, In *Proc. 8th Workshop on RF Supercond.* [25], pages 814–821.

[3] E. Kako et al., Cavity performance in the 1.3 GHz Saclay/KEK Nb cavities, In *Proc. 8th Workshop on RF Supercond.* [25], pages 491–502.

[4] E. Kako et al., Improvement of cavity performance in the Saclay/Cornell/DESY cavities, these proceedings.

[5] E. Kako et al., Improvement of cavity performance by electropolishing in the 1.3 GHz Nb superconducting cavities, in *Proc. 1999 Part. Accel. Conf.*, pages 432–434, New York, NY, 1999.

[6] M. Ono et al., Achievement of 40 MV/m accelerating field in L-band scc at KEK, In *Proc. 8th Workshop on RF Supercond.* [25], pages 472–484.

[7] C. Antoine, (CEA Saclay) private communication.

[8] K. Saito et al., Superiority of electropolishing over chemical polishing on high gradients, In *Proc. 8th Workshop on RF Supercond.* [25], pages 795–813.

[9] R. L. Geng, J. Knobloch, and H. Padamsee, Microstructures of rf surfaces in the electron-beam-weld regions of niobium, these proceedings.

[10] A. C. Rose-Innes and E. H. Rhoderick, *Introduction to Superconductivity*, Pergamon Press, Glasgow, Scotland, 1969.

[11] F. Kœchlin and B. Bonin, *Superconductor Science and Technology* **9**, 453 (1996).

[12] J. Halbritter, *Zeitschrift der Physik* **238**, 466 (1970).

[13] R. M. Scanlan, Properties of conductors, normal and superconducting, in *Handbook of Accelerator Physics and Engineering*, edited by A. W. Chao and M. Tigner, pages 361–365, World Scientific, 1998.

[14] K. Mittag, *Cryogenics* **13**, 94 (1973).

[15] H. Padamsee, Heat transfer and models for breakdown, in *Proc. Workshop RF Supercond.*, edited by M. Kuntze, pages 145–189, Karlsruhe, Germany, 1980, Proceedings also published as internal Kernforschungszentrum Kalsruhe report KFK-3019.

[16] J. H. Graber, *High Power Processing Studies of 3 GHz Niobium Superconducting Accelerator Cavities*, PhD thesis, Cornell University, 1993, Laboratory of Nuclear Studies thesis CLNS 93-1.

[17] F. L. Palmer, *Influence of Oxide Layers on the Microwave Surface Resistance of Superconducting Niobium*, PhD thesis, Cornell University, 1988.

[18] W. DeSorbo, *Phys. Rev.* **132**, 107 (1963).

[19] T. Hays and H. Padamsee, Response of superconducting cavities to high peak power, in *Proc. 1995 Part. Accel. Conf.*, pages 1617–1619, Dallas, TX, 1995.

[20] T. Hays, (Cornell University) private communication.

[21] J. Knobloch and R. Freyman, Effect of high-pressure rinsing on niobium, Technical report, Cornell University, Laboratory of Nuclear Studies, 1998, SRF report 980223-01.

[22] J. Knobloch, *Advanced Thermometry Studies of Superconducting RF Cavities*, PhD thesis, Cornell University, 1997, Laboratory of Nuclear Studies thesis CLNS 97-3.

[23] E. Kako, (KEK, Japan) private communication.

[24] R. W. Röth, H.-G. Kürschner, G. Müller, H. Piel, and D. Reschke, Thermal stability of superconducting Nb cavities at 3 GHz, in *Proc. 3rd Europ. Part. Accel. Conf.*, edited by H. Henke, H. Homeyer, and C. Petit-Jean-Genaz, pages 1325–1327, Berlin, Germany, 1992.

[25] *Proc. 8th Workshop on RF Supercond.*, Padua, Italy, 1997.